Contribution from the Laboratoire de Synthèse et d'Electrosynthèse, Organométallique Associe au CNRS (LA 33), Université de Dijon, Faculte des Sciences "Gabriel", 21100 Dijon, France, and Department of Chemistry, University of Houston—University Park, Houston, Texas 77004

Electrochemistry and Spectroelectrochemistry of σ-Bonded Aryliron Porphyrins. 3. Synthesis and Characterization of High, Low, and Variable Spin State Five-Coordinate σ-Bonded Aryl- and Perfluoroaryliron(III) Complexes[1]

R. GUILARD,*[2a] B. BOISSELIER-COCOLIOS,[2b] A. TABARD,[2a] P. COCOLIOS,†[2b] B. SIMONET,[2b] and K. M. KADISH*[2b]

Received January 2, 1985

The syntheses of 10 novel high- and low-spin σ-bonded aryliron(III) porphyrins are reported and their electrochemical behaviors characterized in benzonitrile containing 0.1 M tetrabutylammonium hexafluorophosphate as supporting electrolyte. Each neutral complex was also characterized by ^1H NMR, ESR, IR, and UV–visible spectroscopy, and on the basis of these data, the spin state of the Fe(III) was assigned as either high-spin $S = {}^5/_2$ or low-spin $S = {}^1/_2$. σ-Bonded Fe(III) porphyrins have generally been described as low-spin species, and an assignment of high-spin Fe(III) at room temperature has never been reported in the literature. Comparisons are made between the redox reactivity and physicochemical properties of these new complexes and results already reported in the literature for low-spin σ-bonded phenyl- and alkyliron(III) porphyrins. Finally, it is demonstrated how the spin state of the σ-bonded aryliron(III) porphyrins and the chemical and electrochemical reactivity can be varied as a function of the porphyrin ring basicity and/or the ligand field strength of the σ-bonded ligand.

Introduction

A considerable amount of the recent research activity has concentrated on the characterization and reactivity of synthetic[3–20] and naturally occurring[21,25] σ-bonded alkyl- or aryliron(III) porphyrins. A number of model compounds have been investigated and, when combined with in vivo experiments,[21–25] have provided proof that the formation of cytochrome P-450 complexes involves an iron–carbon-bonded species upon the metabolic reduction of derivatives like polyhalogenated compounds.

The iron–carbon σ bond introduces very unusual electronic and structural properties to the metalloporphyrin unit. For example, in solution (P)Fe(R) (where P is a porphyrin and R = an alkyl or aryl group) are generally described as five-coordinate, low-spin iron(III) derivatives.[3–20] However, by lowering the temperature in noncoordinating solvents (such as toluene or benzene), the presence of a spin equilibrium has been observed.[26] In addition, electrochemical measurements indicate dramatic cathodic shifts of half-wave potentials for both the oxidation and reduction of the low-spin Fe(III) complexes with respect to the corresponding high-spin (P)FeX derivatives (where X is an anionic ligand) in the same media.[3,4,10,12,27]

It is well established that the spin state of an Fe(III) porphyrin is dependent on the ligand field strength of the axial[28–31] and equatorial (porphyrin)[32–34] ligands. The more basic the porphyrin macrocycle, the higher the spin multiplicity. Variation in the porphyrin ligand and/or axial ligand may also result in a spin state equilibrium for Fe(III).[34–36] Generally, the high-spin state ($S = {}^5/_2$) arises in five-coordinate ferric porphyrins with a single moderate- or weak-field axial ligand. In contrast, the low-spin state ($S = {}^1/_2$) is generally observed for six-coordinate ferric porphyrins having two strong- or moderate-field ligands.[28–30]

Recently, a direct correlation was demonstrated between the spin state of (porphinato)iron(III) complexes and the degree of porphyrin ligand basicity.[34] In this study, half-wave potentials for reduction of 12 different free-base porphyrins were taken as a measure of the porphyrin-ring basicity. These reversible values of $E_{1/2}$ were then plotted vs. the measured magnetic moment of iron(III) in the six-coordinate $[(P)Fe(3\text{-}ClPy)_2]^+ClO_4^-$ species having the same porphyrin ring as the free-base porphyrin. A linear slope of $E_{1/2}$ vs. μ_{eff} was obtained in $CHCl_3$ or CH_3NO_2, and from this correlation, it was concluded that the magnetic moment of Fe(III) was directly dependent upon the porphyrin-ring basicity.

The above study is an excellent first step in the control and prediction of Fe(III) porphyrin spin state. In this paper we have extended this concept of "spin state tuning" by investigating relationships between the axial and equatorial (macrocyclic) ligands of a given Fe(III) porphyrin, the spin state of the complex in

† Present address: L'Air Liquide, CRCD, F-78350 Jouy-en-Josas, France.

(1) For parts 1 and 2 of this series, see ref 3 and 4.
(2) (a) Université de Dijon. (b) University of Houston—University Park.
(3) Lançon, D.; Cocolios, P.; Guilard, R.; Kadish, K. M. *J. Am. Chem. Soc.* **1984**, *106*, 4472.
(4) Lançon, D.; Cocolios, P.; Guilard, R.; Kadish, K. M. *Organometallics* **1984**, *3*, 1164.
(5) Clarke, D. A.; Dolphin, D.; Grigg, R.; Johnson, A. W.; Pinnock, H. A. *J. Chem. Soc. C* **1968**, 881.
(6) Reed, C. A.; Mashiko, T.; Bentley, S. P.; Kastner, M. E.; Scheidt, W. R.; Spartalian, K.; Lang, G. *J. Am. Chem. Soc.* **1979**, *101*, 2948.
(7) Lexa, D.; Saveant, J. M.; Battioni, J. P.; Lange, M.; Mansuy, D. *Angew. Chem., Int. Ed. Engl.* **1981**, *20*, 578.
(8) Brault, D.; Bizet, C.; Morliere, P.; Rougee, M.; Land, E. J.; Santus, R.; Swallow, A. J. *J. Am. Chem. Soc.* **1980**, *102*, 1015.
(9) Brault, D.; Neta, P. *J. Am. Chem. Soc.* **1981**, *103*, 2705.
(10) Lexa, D.; Mispelter, J.; Saveant, J. M. *J. Am. Chem. Soc.* **1981**, *103*, 6806.
(11) Ortiz de Montellano, P. R.; Kunze, K. L.; Augusto, O. *J. Am. Chem. Soc.* **1982**, *104*, 3545.
(12) Lexa, D.; Saveant, J. M. *J. Am. Chem. Soc.* **1982**, *104*, 3503.
(13) Cocolios, P.; Laviron, E.; Guilard, R. *J. Organomet. Chem.* **1982**, *228*, C39.
(14) Ogoshi, H.; Sugimoto, H.; Yoshida, Z.; Kobayashi, H.; Sakai, H.; Maeda, Y. *J. Organomet. Chem.* **1982**, *234*, 185.
(15) Mansuy, D.; Battioni, J. P. *J. Chem. Soc., Chem. Commun.* **1982**, 638.
(16) Mansuy, D.; Fontecave, M.; Battioni, J. P. *J. Chem. Soc., Chem. Commun.* 1982, 317.
(17) Mansuy, D.; Battioni, J. P.; Dupre, D.; Sartori, E. *J. Am. Chem. Soc.* **1982**, *104*, 6159.
(18) Cocolios, P.; Lagrange, G.; Guilard, R. *J. Organomet. Chem.* **1983**, *253*, 65.
(19) Kunze, K. L.; Ortiz de Montellano, P. R. *J. Am. Chem. Soc.* **1983**, *105*, 1380.
(20) Battioni, P.; Mahy, J. P.; Gillet, G.; Mansuy, D. *J. Am. Chem. Soc.* **1983**, *105*, 1399.
(21) Mansuy, D.; Nastainczyk, W.; Ullrich, V. *Arch. Pharmakol.* **1974**, *285*, 315.
(22) Wolf, C. R.; Mansuy, D.; Nastainczyk, W.; Deutschmann, G.; Ullrich, V. *Mol. Pharmacol.* **1977**, *13*, 698.
(23) Nastainczyk, W.; Ullrich, V.; Sies, H. *Biochem. Pharmacol.* **1978**, *27*, 387.
(24) Ahr, H. J.; King, L. J.; Nastainczyk, W.; Ullrich, V. *Biochem. Pharmacol.* **1982**, *31*, 383.
(25) Augusto, O.; Kunze, K. L.; Ortiz de Montellano, P. R. *J. Biol. Chem.* **1982**, *257*, 6231.
(26) Tabard, A.; Cocolios, P.; Lagrange, G.; Geravdin, R.; Hubsch, J.; Lecomte, C.; Zarembowitch, J.; Guilard, R., submitted for publication.
(27) Kadish, K. M. *J. Electroanal. Chem.* **1984**, *168*, 261.
(28) Scheidt, W. R.; Reed, C. A. *Chem. Rev.* **1981**, *81*, 543.
(29) Scheidt, W. R.; Geiger, D. K.; Hayes, R. G.; Lang, G. *J. Am. Chem. Soc.* **1983**, *105*, 2625.

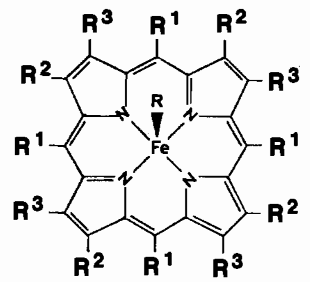

Name	R group	R1	R2	R3
(OEP)Fe(C_6F_4H)	C_6F_4H	H	Et	Et
(TPP)Fe(C_6F_4H)	C_6F_4H	C_6H_5	H	H
((m-Me)TPP)Fe(C_6F_4H)	C_6F_4H	(m-Me)C_6H_4	H	H
((p-Me)TPP)Fe(C_6F_4H)	C_6F_4H	(p-Me)C_6H_4	H	H
(OEP)Fe(C_6F_5)	C_6F_5	H	Et	Et
(TPP)Fe(C_6F_5)	C_6F_5	C_6H_5	H	H
((m-Me)TPP)Fe(C_6F_5)	C_6F_5	(m-Me)C_6H_4	H	H
((p-Me)TPP)Fe(C_6F_5)	C_6F_5	(p-Me)C_6H_4	H	H
((p-Et_2N)TPP)Fe(C_6H_5)	C_6H_5	(p-Et_2N)C_6H_4	H	H
((CN)$_4$TPP)Fe(C_6H_5)	C_6H_5	C_6H_5	H	CN

Figure 1. Schematic representation of the investigated σ-bonded (P)-Fe(R) complexes.

solution, and its chemical and electrochemical reactivity. This has not been done in any previous investigation. Four different types of porphyrin ligands and three different types of σ-bonded aryl and perfluoroaryl groups were utilized in the synthesis of the investigated compounds. Because σ-bonded Fe(III) porphyrins are essential intermediates in a number of biological reactions,[21-25] it is thus of importance to determine the molecular parameters leading to discrete high-spin or low-spin complexes or to a spin equilibria system in solution.

Previous electrochemical studies of σ-bonded porphyrins have concentrated on the reactions of low-spin, five- and six-coordinate OEP and TPP complexes where the σ-bonded ligands were simple alkyl or phenyl groups.[3,4,10,12,13,37] We now report the electrochemistry and characterization of 10 other σ-bonded iron(III) porphyrins where the iron(III) is either discretely low spin ($S = {}^1/_2$), is discretely high spin ($S = {}^5/_2$), or has one spin state or the other according to the selected experimental conditions.

A schematic representation of the investigated σ-bonded Fe(III) porphyrins and the substituents on the porphyrin ring is shown in Figure 1. The investigated compounds can be broken into three logical groups according to the nature of the Fe(III) spin state: (i) the σ-bonded perfluoroaryliron(III) complexes, (P)Fe(C_6F_4X) [X = H, F; P = OEP, TPP, (*m*-Me)TPP, (*p*-Me)TPP]; (ii) the σ-bonded phenyliron(III) (diethylamino)tetraphenylporphyrin complex, ((p-Et_2N)TPP)Fe(C_6H_5); (iii) the tetracyano-substituted σ-bonded phenyl complex, ((CN)$_4$TPP)Fe(C_6H_5). These three series of compounds are shown schematically.

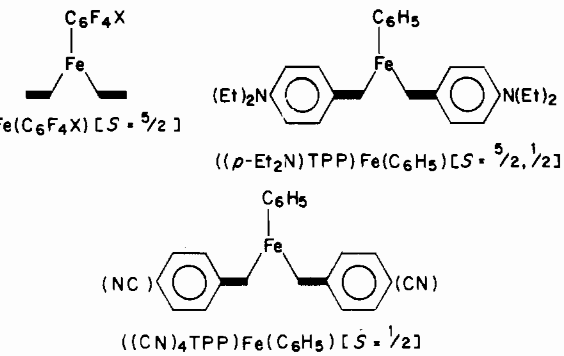

The first and last series of compounds (i and iii) exist as high- and low-spin complexes, respectively, while the middle compound (ii) may exist in the high or low spin state, depending upon the experimental conditions. On the basis of data for the above series of complexes, we will demonstrate how the spin state and the reactivity of σ-bonded iron(III) porphyrins vary as a function of the porphyrin ring basicity and/or the ligand field strength of the σ-bonded ligands. To our knowledge, the iron(III) σ-bonded porphyrins investigated in this paper represent the first iron(III) porphyrinic series for which such spin state tuning is possible.

Experimental Section

Chemicals. The synthesis and handling of the σ-aryliron porphyrins was carried out under an argon atmosphere. All common solvents were thoroughly dried in an appropriate manner and were distilled under argon prior to use. All operations were achieved in Schlenk tubes under purified argon, using dried oxygen-free solvents. The Fe(III) porphyrins, (OEP)FeCl,[38] (TPP)FeCl,[38] ((*m*-Me)TPP)FeCl,[38] ((*p*-Me)TPP)FeCl,[38] ((*p*-Et_2N)TPP)FeCl,[39] and ((CN)$_4$TPP)FeCl[40] were synthesized by literature methods. For the electrochemical studies, methylene chloride (CH_2Cl_2) was distilled from CaH_2 while benzonitrile (PhCN) was distilled from P_2O_5 under reduced pressure prior to use. Tetrabutylammonium hexafluorophosphate ((TBA)PF_6) was recrystallized from methylene chloride/hexane mixtures. The perfluoroaryl- and aryliron porphyrins, (P)Fe(C_6F_4X), ((*p*-Et_2N)TPP)Fe(C_6H_5), and ((CN)$_4$TPP)Fe(C_6H_5), were prepared by the action of an organomagnesium compound on the respective porphyrin iron(III) chloride, (P)Fe(Cl). Detailed procedures for the preparation of (P)Fe(C_6F_4X), ((*p*-Et_2N)TPP)Fe(C_6H_5), and ((CN)$_4$TPP)Fe(C_6H_5) are given below:

General Procedures for Preparation of the σ-Bonded Perfluoroaryl Derivatives, (P)Fe(C_6F_4X). One equivalent of perfluorophenylmagnesium bromide in toluene was added dropwise in the dark to 0.7 mmol of (P)Fe(Cl) in 450 mL of toluene. The reaction was monitored by TLC (using benzene as eluent and basic aluminum oxide) and stopped after 48 h. The reaction mixture was hydrolyzed with 20 mL of deaerated distilled water after which the organic layer was washed with water until neutrality and then dried over $MgSO_4$. After filtration, the toluene solution was evaporated under reduced pressure and chromatographed in the dark over a basic alumina-packed column in an argon atmosphere using benzene as eluent. The obtained product was recrystallized from benzene/heptane, and the yield of the reaction was close to 50%.

Synthesis of ((*p*-Et_2N)TPP)Fe(C_6H_5) and ((CN)$_4$TPP)Fe(C_6H_5). A benzene solution of phenylmagnesium bromide was added dropwise via a syringe to 250 mg of ((*p*-Et_2N)TPP)Fe(Cl) (0.25 mmol) in 80 mL of freshly distilled benzene, and completion of the reaction was monitored by TLC (using neutral aluminum oxide and 1:1 toluene/CH_2Cl_2 as eluent). The iron–phenyl complex eluted first and formed an orange spot that was unstable in the open air. The starting material was seen as a green spot (due to the transformation of (P)Fe(Cl) to the μ-oxo dimer on the aluminum oxide plate). The reaction medium was hydrolyzed with 20 mL of deaerated distilled water, and the two layers were separated. The organic layer was washed twice with water and then dried over Na_2SO_4 for 2 h in the dark. After filtration, the benzene solution was rapidly passed through a short column of basic alumina with a 200:1 mixture of benzene/acetone as eluent. The solvent was removed by

(30) Scheidt, W. R.; Geiger, D. K.; Haller, K. J. *J. Am. Chem. Soc.* **1982**, *104*, 495.
(31) Behere, D. V.; Birdy, R.; Mitra, S. *Inorg. Chem.* **1984**, *23*, 1978.
(32) Mitra, S. In "Iron Porphyrins"; Lever, A. B. P., Gray, H. B., Eds.; Addison-Wesley: Reading MA, 1983; Part II, Chapter 1.
(33) Scheidt, W. R.; Lee, J. Y.; Geiger, D. K.; Taylor, K.; Hatano, K. *J. Am. Chem. Soc.* **1982**, *104*, 3367.
(34) Geiger, D. K.; Scheidt, W. R. *Inorg. Chem.* **1984**, *23*, 1970.
(35) Hill, A. O.; Morallee, K. G. *J. Am. Chem. Soc.* **1972**, *94*, 731.
(36) Kadish, K. M.; Su, C. H. *J. Am. Chem. Soc.* **1983**, *105*, 177.
(37) Kadish, K. M.; Lancon, D.; Cocolios, P.; Guilard, R. *Inorg. Chem.* **1984**, *23*, 2372.
(38) Buchler, J. W. In "The Porphyrins"; Dolphin, D., Ed.; Academic Press: New York, 1978; Vol. I, Chapter 10 and references therein.
(39) Walker, F. A.; Balke, V. L.; McDermott, G. A. *J. Am. Chem. Soc.* **1982**, *104*, 1569.
(40) Giraudeau, A.; Callot, H. J.; Jordan, J.; Ezhar, I.; Gross, M. *J. Am. Chem. Soc.* **1979**, *101*, 3857.

Table I. Elemental Analysis[a] and Mass Spectral Data of the Investigated (P)Fe(R) Complexes

compd	molec formula	% C	% H	% N	% F	% Fe	fragment	m/e (%)
(OEP)Fe(C_6F_4H)	$C_{42}H_{45}N_4F_4Fe$	68.5	6.2	7.4	10.1	7.5	$[(OEP)Fe]^+$	588 (100)
		(68.38)	(6.16)	(7.59)	(10.30)	(7.57)	$[(OEP)Fe(C_6F_4H)^{+\cdot}$	738 (22)
(TPP)Fe(C_6F_4H)	$C_{50}H_{29}N_4F_4Fe$	73.3	3.4	6.9	9.5	6.6	$[(TPP)Fe]^+$	668 (100)
		(73.44)	(3.58)	(6.85)	(9.30)	(6.83)	$[(TPP)Fe(C_6F_4H)]^{+\cdot}$	819 (19)
((*m*-Me)TPP)Fe(C_6F_4H)	$C_{54}H_{37}N_4F_4Fe$	74.2	4.1	6.5	8.6	6.5	$[((m\text{-Me})TPP)Fe]^+$	724 (100)
		(74.22)	(4.28)	(6.41)	(8.70)	(6.39)	$[((m\text{-Me})TPP)Fe(C_6F_4H)]^{+\cdot}$	874 (30)
((*p*-Me)TPP)Fe(C_6F_4H)	$C_{54}H_{37}N_4F_4Fe$	74.1	4.4	6.3	8.6	6.5	$[((p\text{-Me})TPP)Fe]^+$	724 (100)
		(74.22)	(4.28)	(6.41)	(8.70)	(6.39)	$[((p\text{-Me})TPP)Fe(C_6F_4H)]^{+\cdot}$	874 (22)
(OEP)Fe(C_6F_5)	$C_{42}H_{44}N_4F_5Fe$	66.6	5.7	7.4	12.6	7.3	$[(OEP)Fe]^+$	588 (100)
		(66.75)	(5.88)	(7.41)	(12.57)	(7.39)	$[(OEP)Fe(C_6F_5)]^{+\cdot}$	756 (21)
(TPP)Fe(C_6F_5)	$C_{50}H_{28}N_4F_5Fe$	71.9	3.2	6.6	11.4	6.7	$[(TPP)Fe]^+$	668 (100)
		(71.86)	(3.38)	(6.70)	(11.37)	(6.68)	$[(TPP)Fe(C_6F_5)]^{+\cdot}$	836 (22)
((*m*-Me)TPP)Fe(C_6F_5)	$C_{54}H_{36}N_4F_5Fe$	72.7	4.0	6.4	10.6	6.4	$[((m\text{-Me})TPP)Fe]^+$	724 (100)
		(72.73)	(4.08)	(6.28)	(10.65)	(6.26)	$[((m\text{-Me})TPP)Fe(C_6F_5)]^{+\cdot}$	892 (30)
((*p*-Me)TPP)Fe(C_6F_5)	$C_{54}H_{36}N_4F_5Fe$	72.6	4.2	6.1	10.6	6.1	$[((p\text{-Me})TPP)Fe]^+$	724 (100)
		(72.73)	(4.08)	(6.28)	(10.65)	(6.26)	$[((p\text{-Me})TPP)Fe(C_6F_5)]^{+\cdot}$	892 (25)
((*p*-Et_2N)TPP)Fe(C_6H_5)	$C_{66}H_{69}N_8Fe$	76.9	6.8	10.7		5.3	$[((p\text{-}Et_2N)TPP)Fe]^+$	953 (98)
		(76.94)	(6.76)	(10.87)		(5.42)	$[((p\text{-}Et_2N)TPP)Fe\text{–}H]^+$	952 (100)
((CN)$_4$TPP)Fe(C_6H_5)	$C_{54}H_{29}N_8Fe$	76.5	3.6	13.4		6.8	$[((CN)_4TPP)Fe\text{–}CN]^+$	743 (100)
		(76.69)	(3.46)	(13.24)		(6.60)	$[((CN)_4TPP)Fe]^+$	769 (86)
							$[((CN)_4TPP)Fe(C_6H_5)\text{–}CN]^+$	820 (23)
							$[((CN)_4TPP)Fe(C_6H_5)]^{+\cdot}$	845 (9)

[a] Calculated values in parentheses.

evaporation under reduced pressure, and 125 mg of ((*p*-Et_2N)TPP)Fe(C_6H_5) was obtained; yield 48%.

Synthesis of ((CN)$_4$TPP)Fe(C_6H_5) was carried out from ((CN$_4$)TPP)FeCl in a manner similar to that described for ((*p*-Et_2N)TPP)Fe(C_6H_5). The yield for this reaction was close to 40%.

Instrumentation. Elemental analyses were performed by the Service de Microanalyse du CNRS. Mass spectra were recorded in the electron-impact mode with a Finnigan 3300 spectrometer: ionizing energy 30–70 eV; ionizing current 0.4 mA; source temperature 250–400 °C. ^1H NMR spectra were recorded on a Brucker WM 400 of the Cerema (Centre de Resonance Magnetique of the University of Dijon). Spectra were measured from 5-mg solutions of complex in C_6D_6 with tetramethylsilane as internal reference. ESR spectra were recorded at 115 K in toluene on either a Varian E4 X-band spectrometer or an IBM Model ER 100 D spectrometer equipped with a microwave ER-040-X bridge and an ER 080 power supply. The *g* values were measured with respect to diphenylpicrylhydrazyl ($g = 2.0036 \pm 0.0003$). Infrared spectra were obtained on a Perkin-Elmer 580 B apparatus. Samples were prepared as either 1% dispersions in CsI pellets or Nujol mulls. Electronic absorption spectra were recorded on a Perkin-Elmer 559 spectrophotometer, a Tracor Northern 1710 holographic optical spectrometer–multichannel analyzer, or an IBM Model 9430 spectrophotometer.

Cyclic voltammetry was carried out with either an EG&G Model 173 potentiostat and an EG&G Model 175 Universal Programmer, on an IBM instruments Model EC 225 voltammetric analyzer or on a BAS 100 electrochemical analyzer. Current–voltage curves were recorded on a Houston Instruments Model 2000 X-Y recorder or a Houston Instruments HIPLOT DMP-40 plotter and an EPSON Model FX80 printer. A three-electrode system was used with a Pt-button working electrode, a Pt-wire counter electrode, and a saturated calomel electrode (SCE) as reference. The reference electrode was separated from the bulk of the solution by a fritted-glass bridge filled with the solvent and supporting electrolyte. Solutions of electrolyte were deoxygenated by a solvent-saturated stream of nitrogen for at least 10 min before introduction of the porphyrin and were protected from air by a nitrogen blanket during the experiment.

Bulk controlled-potential electrolysis was performed in a specially constructed cell where the SCE reference electrode and the platinum-wire counter electrode were separated from the test solution by fritted bridges containing solvent and supporting electrolyte. A BAS 100 electrochemical analyzer was used to control the potentials. Spectroelectrochemical experiments and thin-layer coulometry or electrolysis were performed at a platinum thin-layer electrode[41] or an optically transparent gold thin-layer electrode (OTTLE) that has been described previously.[42] Potentials were monitored with an IBM Instruments Model EC 225 voltammetric analyzer, and time-resolved UV-visible spectra were recorded with a Tracor Northern 1710 holographic optical spectrometer/multichannel analyzer.

(41) Lin, X.; Kadish, K. M. *Anal. Chem.* **1985**, *57*, 1498.
(42) Rhodes, R. K.; Kadish, K. M. *Anal. Chem.* **1981**, *53*, 1539.

Table II. IR Data of the Investigated (P)Fe(R) Complexes

R	porphyrin, P	ν, cm^{-1}						
C_6F_4H	OEP	1322	1160	1085	884	675		250
	TPP	1327		1085	885	670		272
	(*m*-Me)TPP	1328	1160		885	678		262
	(*p*-Me)TPP	1330	1163	1088	886	678		268
C_6F_5	OEP	1630	1503	1433	952	645		245
	TPP	1632	1508	1429	957	662		272
	(*m*-Me)TPP	1632	1504	1432	955	662		262
	(*p*-Me)TPP	1631	1500	1430	953	668		268
C_6H_5	(*p*-Et_2N)TPP		1555	1462	723	682		
	(CN$_4$)TPP	2218	1554					398
	OEP	1556	1418	1007	720	680	641	368
	TPP	1554	1420	720	682	670	464	342

Results and Discussion

Characterization of Neutral (P)Fe(R) Complexes. Elemental analysis and mass spectral data of the 10 investigated σ-aryliron(III) porphyrins are given in Table I and suggest the molecular formula (P)Fe(R) for the obtained products. For the case of ((CN)$_4$TPP)Fe(C_6H_5), the observed parent peak in the mass spectrum is $[(P)Fe - CN]^+$, while for all other complexes the base peak corresponds to the ionic species $[(P)Fe]^+$. The intensity of the molecular peak is significant for all the derivatives (8–30%) and is in good agreement with the fragmentation patterns generally observed for σ-alkyl (or σ-aryl) metalloporphyrins.[18]

The IR data of 12 (P)Fe(R) complexes are reported in Table II where only the vibrational frequencies not found for the starting (P)Fe(Cl) species are listed. For the perfluoroaryl derivatives (R = C_6F_4H, C_6F_5), the characteristic vibrations of the perfluoroaryl moiety bound to a metal appear in the range of 250–1650 cm^{-1}.[43] The C–H out-of-plane stretching mode of the phenyliron compounds, (P)Fe(C_6H_5), are observed in the region of 600–800 cm^{-1}, and the phenyl-ring deformation stretching frequencies appear between 400 and 500 cm^{-1}. The sharp ν_{C-C} vibrations of ((*p*-Et_2N)TPP)Fe(C_6H_5) and ((CN)$_4$TPP)Fe(C_6H_5) are located close to 1550 cm^{-1}.

The UV–visible spectra of compounds characterized in this study are summarized in Table III. Also included in this table are spectra for the OEP and TPP phenyliron derivatives in PhCN (0.1 M TBAP). The electronic absorption spectra of the eight perfluoro derivatives (R = C_6F_4H, C_6F_5) have a morphology typical of high-spin $S = {}^5/_2$ complexes.[44] For the TPP, or *m*- and

(43) Maslowsky, E., Jr. In "Vibrational Spectra of Organometallic Compounds", 2nd ed.; Wiley: New York, 1978; p 191.

Table III. UV-Visible Data of the Investigated (P)Fe(R) Complexes in Toluene

R	porphyrin, P	λ_{max}, nm ($\epsilon \times 10^{-3}$)				
		Soret region		Q bands		
C_6F_4H	OEP	368 (80)	403 (sh)	508 (9.8)	534 (9.6)	645 (5.3)
	TPP	366 (56)	417 (93)	512 (14.1)		719 (3.3)
	(*m*-Me)TPP	367 (35)	416 (71)	511 (8.7)		718 (2.1)
	(*p*-Me)TPP	368 (57)	418 (104)	513 (14.1)		720 (3.6)
C_6F_5	OEP	386 (51)	395 (sh)	506 (7.2)	535 (6.3)	644 (2.9)
	TPP	366 (51)	417 (91)	512 (12.2)		717 (2.9)
	(*m*-Me)TPP	366 (56)	419 (98)	513 (13.6)		718 (3.3)
	(*p*-Me)TPP	367 (62)	419 (109)	513 (15.6)		721 (3.8)
C_6H_5	(*p*-Et_2N)TPP	406 (sh)	440 (96)		526 (16)	
	$(CN)_4$TPP		437 (94.2)		605 (20.2)	680 (5.3)
	OEP	368 (60)	392 (129)	515 (12.7)	555 (20.8)	
	TPP	389 (19)	408 (93)	518 (7.4)	548 (5.5)	

Table IV. ESR Data of the Investigated (P)Fe(R) Complexes in Toluene at 115 K

R	porphyrin, P	$g_\perp$		$g_\parallel$
C_6F_4H	OEP	5.88		1.98
	TPP	5.86		1.98
	(*m*-Me)TPP	5.86		1.98
	(*p*-Me)TPP	5.81		1.98
C_6F_5	OEP	6.08[a]		1.97[a]
	TPP	5.86		1.99
	(*m*-Me)TPP	5.86		1.98
	(*p*-Me)TPP	5.85		1.98
C_6H_5	(*p*-Et_2N)TPP	5.96		2.02
		g_x	g_y	g_z
C_6H_5	$(CN)_4$TPP	1.97	2.06	2.25

[a] In 2:1 toluene-methylene chloride mixtures.

p-methyl-substituted TPP derivatives, this involves a Soret band located in the region of 415–420 nm while, for the OEP complexes, this band is located close to 370 nm. In addition, all of these compounds exhibit an extra band between 360 and 420 nm that is blue shifted with respect to the Soret band for the tetraarylporphyrin series and red shifted with respect to the Soret band for the two investigated octaethylporphyrin species. The presence of this second band for the σ-bonded perfluoro complexes confers a slight hyper-porphyrin character to these species.[44] All of the perfluoro complexes have Q bands (near 510 nm) that are characteristic of Fe(III) porphyrin entities. In addition, all of the TPP derivatives with bound C_6F_4H or C_6F_5 ligands have a metal → ligand charge-transfer band between 717 and 721 nm.[45]

The above UV–visible data tend to demonstrate that the eight perfluoroaryl complexes possess a high-spin state ($S = {}^5/_2$) in solution. In contrast, the phenyliron OEP and TPP derivatives have UV-visible spectra characteristic of low-spin complexes. A sharp Soret band is located at 392 nm for the OEP complex and at 408 nm for the TPP complex, and both species have two bands between 515 and 555 nm. However, for the two remaining phenyliron complexes, it is impossible to predict the spin state on the basis of their electronic absorption spectra. For the ((*p*-Et_2N)TPP)Fe(C_6H_5) complex, the Soret band is located at 440 nm and a single Q band is located at 526 nm. A shoulder appears on the Soret band at 406 nm. In contrast, the (($(CN)_4$TPP)Fe(C_6H_5) complex has only a single Soret band at 437 nm and two Q bands at 605 and 680 nm.

The ESR spectra of ((*m*-Me)TPP)Fe(C_6F_4H), ((*p*-Et_2N)TPP)Fe(C_6H_5), and ((CN_4)TPP)Fe(C_6H_5) are shown in Figure 2, and a summary of the obtained *g* values for all of the complexes at 115 K in toluene is given in Table IV. As seen in this figure and table, the ESR spectra for 9 of the 10 investigated compounds have an axial symmetry ($g_\perp \simeq 6$; $g_\parallel \simeq 2$), confirming the high-spin, $S = {}^5/_2$, state. In contrast, (($(CN)_4$TPP)Fe(C_6H_5)

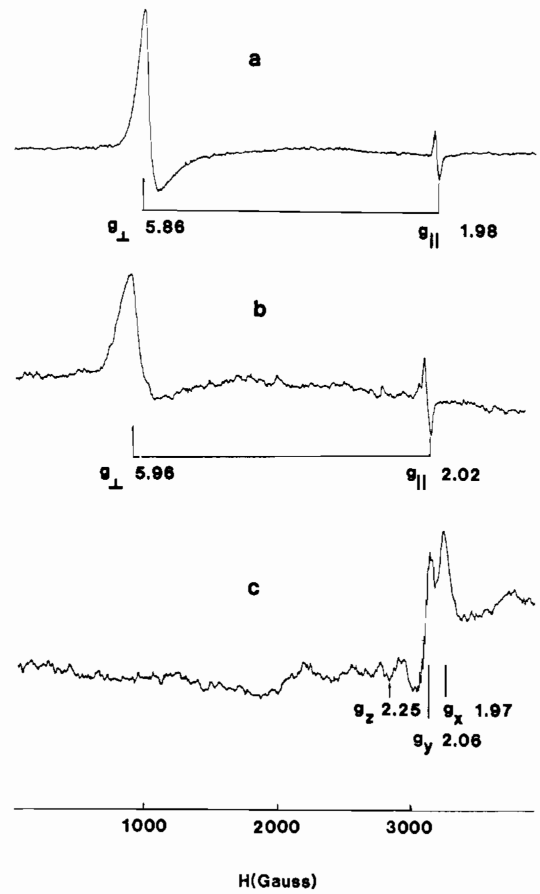

Figure 2. ESR spectra of (a) ((*m*-Me)TPP)Fe(C_6F_4H), (b) ((*p*-Et_2N)TPP)Fe(C_6H_5), and (c) (($(CN)_4$TPP)Fe(C_6H_5), recorded at 115 K in toluene.

exhibits three lines (centered at $g_x = 1.97$, $g_y = 2.06$, and $g_z = 2.25$) that are characteristic of a low-spin, $S = {}^1/_2$ state.

We have observed that the spin state of various iron σ-bonded alkyl and aryl porphyrins depends on numerous parameters such as solvent, method of sample preparation, and temperature.[26] In this present study, we have recorded the ESR spectra of the 10 (P)Fe(R) compounds while varying all of these parameters. For example, CH_2Cl_2 was used as solvent, the samples were diluted in $MgSO_4$, and the spectra were recorded at various temperatures. However, in all cases, the morphology of the spectra was similar to that obtained in toluene at 115 K.

^{1}H NMR Spectroscopy. Figure 3 illustrates the ^{1}H NMR spectra of (OEP)Fe(C_6F_4H) and ((*m*-Me)TPP)Fe(C_6F_5) at 294 K in C_6D_6. These spectra are typical of high-spin $S = {}^5/_2$ species[46] and are consistent with conclusions derived from the above de-

(44) Gouterman, M. In "The Porphyrins"; Dolphin, D., Eds.; Academic Press: New York, 1978; Vol. III, Chapter 1 and references therein.
(45) Makinen, M. W.; Chung, A. K. In "Iron Porphyrins"; Lever, A. B. P., Gray, H. B., Eds.; Addison-Wesley: Reading, MA, 1983; Part I, Chapter 3.

(46) La Mar, G. N.; Walker, F. A. In "The Porphyrins"; Dolphin D., Ed.; Academic Press: New York, 1979; Vol. IV, Chapter 2 and references therein.

Table V. NMR Data[a] of the (P)Fe(R) Complexes

				protons								
				R^1			R^2			R		
R	porphyrin, P	R^1	R^2 (R^3)		m/i[b]	δ		m/i	δ		m/i	δ
C_6F_4H	OEP	H	Et		s/4	−48.56	β-CH_3	s/24	5.88		s/1	−58.85
							α-CH_2	s/8	39.91			
							α′-CH_2	s/8	42.89			
	TPP	C_6H_5	H	o-H	s/4	5.31		s/8	61.18		s/1	−61.47
				o′-H	s/4	8.05						
				m-H	s/4	10.31						
				m′-H	s/4	11.05						
				p-H	s/4	6.18						
	(m-Me)TPP	(m-Me)C_6H_4	H	o-H	s/4	5.11		s/8	61.74		s/1	−61.48
				o′-H	s/4	8.10						
				m-H	s/2	10.28						
				m′-H	s/2	11.07						
				m-Me	s/6	1.98						
				m′-Me	s/6	2.22						
				p-H	s/4	6.04						
	(p-Me)TPP	(p-Me)C_6H_4	H	o′-H	s/4	7.96		s/8	61.94		s/1	−61.11
				m-H	s/4	10.39						
				m′-H	s/4	11.14						
				p-Me, o-H	s/16	5.06						
C_6F_5	OEP	H	Et		s/4	55.01	β-CH_3	s/24	6.19			
							α-CH_2	s/8	41.71			
							α′-CH_2	s/8	42.69			
	TPP	C_6H_5	H	o-H	s/4	5.29		s/8	66.28			
				o′-H	s/4	8.45						
				m-H	s/4	10.67						
				m′-H	s/4	11.48						
				p-H	s/4	6.15						
	(m-Me)TPP	m-MeC_6H_4	H	o-H	s/4	5.16		s/8	66.51			
				o′-H	s/4	8.45						
				m-H	s/2	10.63						
				m′-H	s/2	11.49						
				m-Me	s/6	2.02						
				m′-Me	s/6	2.35						
				p-H	s/4	6.02						
	(p-Me)TPP	p-MeC_6H_4	H	o′-H	s/4	8.29		s/8	66.62			
				m-H	s/4	10.75						
				m′-H	s/4	11.52						
				p-Me, o-H	s/16	5.36						
C_6H_5	(p-Et_2N)TPP	(p-Et_2N)C_6H_4	H	o-H	s/4	3.02		s/8	−16.26	o-H	s/2	−78.21
				o′-H	s/4	4.80				p-H	s/1	−24.51
				m-H	s/4	3.95				m-H	s/2	13.57
				m′-H	s/4	4.20						
				N-CH_2	s/16	1.88						
				CH_3	s/24	0.03						
	$(CN)_4$TPP	C_6H_5	CN(H)	o-H	s/4	3.48		s/4	−19.92	o-H	s/2	−87.96
				o′-H	s/4	5.22				p-H	s/1	−41.07
				m-H	s/4	4.40				m-H	s/2	11.65
				m′-H	s/4	4.96						
				p-H	s/4	5.73						

[a] Spectra recorded in C_6D_6 at 21 °C with $SiMe_4$ as internal reference; chemical shifts downfield from $SiMe_4$ are defined as positive. [b] m = multiplicity; i = intensity; s = singlet.

scribed ESR spectra. NMR spectra characteristic of high-spin Fe(III) porphyrins were also observed for the other perfluoro derivatives. This is shown in Table V which summarizes the NMR data for each of the 10 investigated compounds.

The two octaethylporphyrin derivatives have an out-of-plane iron atom, as clearly demonstrated by the splitting of the α-CH_2 peaks. This morphology is systematically observed for the corresponding chloroiron(III) porphyrins and is typical for high-spin species.[47,48] In accordance with this observation, the meso protons of (OEP)Fe(C_6F_5) and (OEP)Fe(C_6F_4H) give a broad high-field signal in the range of −48 to −56 ppm. In contrast, the pyrrole proton signals of the tetraarylporphyrin derivatives appear at higher fields (+61 to +67 ppm) than those observed for the same proton groups in the corresponding halide complexes.[47,49] This observation is in good agreement with the general properties of the polyfluoroaryl organometallic derivatives that show quite

(47) Walker, F. A.; La Mar, G. N. *Ann. N.Y. Acad. Sci.* **1973**, *206*, 328.

(48) Goff, H. M. In "Iron Porphyrins"; Lever, A. B. P., Gray, H. B., Eds.; Addison-Wesley: Reading, MA, 1983; Part I, Chapter 3.

(49) La Mar, G. N.; Eaton, G. R..; Holm, R. H.; Walker, F. A. *J. Am. Chem. Soc.* **1973**, *95*, 63.

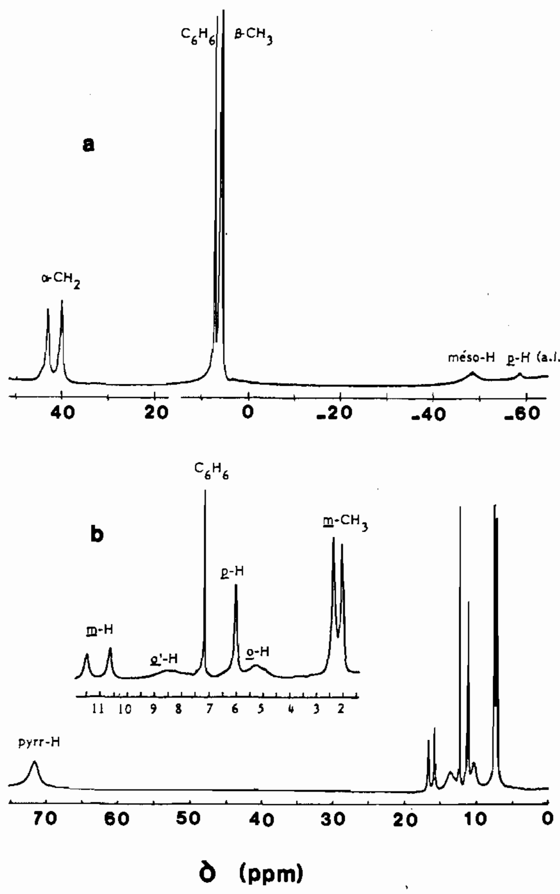

Figure 3. ^{1}H NMR spectra of (a) (OEP)Fe(C_6F_4H) and (b) ((*m*-Me)TPP)Fe(C_6F_5), recorded at 294 K in C_6D_6.

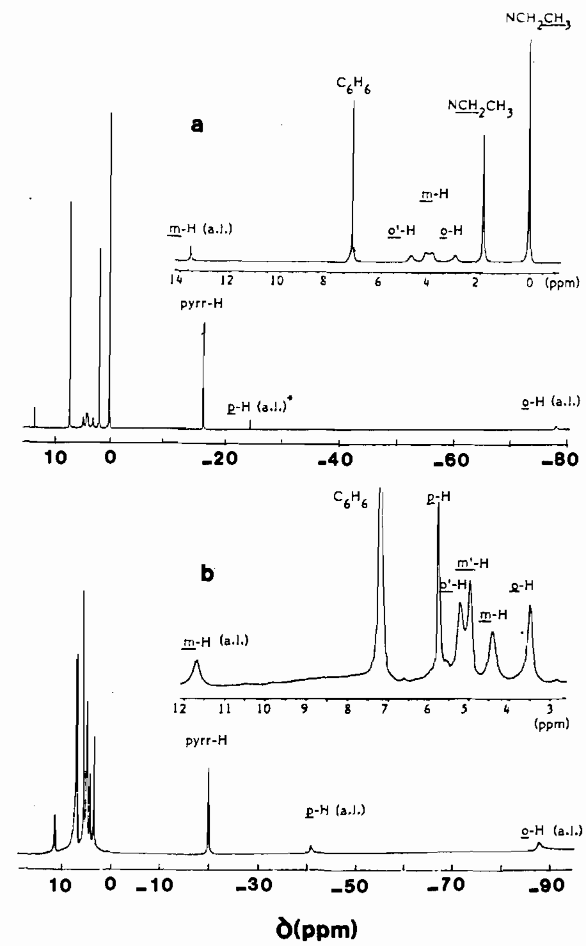

Figure 4. ^{1}H NMR spectra of (a) ((*p*-Et_2N)TPP)Fe(C_6H_5) and (b) ((CN)$_4$TPP)Fe(C_6H_5), recorded at 294 K in C_6D_6.

different magnetic properties.[50] More specifically, the ionic character of the metal–halide bond is more pronounced than that of the metal–carbon bond for these complexes. For the tetraaryl compounds, assignment of the ortho, meta, and para protons was made on the basis of the relative signal intensity and by comparison with the NMR spectra of the TPP, (*m*-Me)TPP, and (*p*-Me)TPP Fe(III) series.[46,49,51] The para protons exhibit a signal around 6.0 ppm while the meta and ortho protons give four signals. The meta proton signals are well separated in the region of 10.3–11.5 ppm, and broad peaks attributable to the ortho protons appear in the range 5.0–8.5 ppm. These results clearly demonstrate that the iron atom is out of the macrocyclic plane since the ortho and meta protons are highly anisotropic in the limit of the slow phenyl-group rotation.[47] The same observations were made for the σ-alkyl- or σ-aryliron(III) derivatives.[18]

Strong resonance signals are observed for Fe(III) porphyrins bound with C_6F_4H. These occur at −58.85 ppm for the octaethylporphyrin systems and in the range −61.1 to +61.5 ppm for the tetraphenylporphyrin series. By comparison with the *p*-H resonance signal of a phenyl σ bonded to an iron porphyrin,[18] a shielding of the *p*-H of the C_6F_4H moiety occurs. This shielding is attributable to the electron-withdrawing character of the perfluoro ligand which induces a metal to axial ligand charge transfer. A comparison of the C_6F_4H and C_6F_5 derivatives shows that the pyrrole proton peaks of pentafluoro complexes are more deshielded. This observation is in good agreement with the nature of the axial ligand; the more electron withdrawing the axial ligand, the lower the field of the pyrrole protons ($C_6F_4H \leq C_6F_5 \leq Cl$). Finally, the ^{1}H NMR spectra of the perfluoro complexes do not show significant modification by varying the temperature. All of these results clearly indicate that the perfluoroaryl iron(III) porphyrins are pure high spin state species. This is not the case for the ((*p*-Et_2N)TPP)Fe(C_6H_5) and ((CN)$_4$TPP)Fe(C_6H_5) complexes.

Figure 4 reproduces the ^{1}H NMR spectra of ((*p*-Et_2N)TPP)Fe(C_6H_5) and ((CN)$_4$TPP)Fe(C_6H_5) at 294 K in C_6D_6. Curiously, the NMR spectrum of ((*p*-Et_2N)TPP)Fe(C_6H_5) is typical of a low-spin iron(III) complex. The pyrrole protons signals are at a high-field position (−16.26 ppm) as compared with the pure high-spin complexes that have the pyrrole signals around +80 ppm. The axial ligand signals of ((*p*-Et_2N)TPP)Fe(C_6H_5) appear as three singlets located at −78.21 ppm (*o*-H), −24.51 ppm (*p*-H), and +13.57 ppm (*m*-H), and the line width is logically increased with respect to the distance of the protons from the paramagnetic center. The phenyl and ethyl protons are shielded as compared to a diamagnetic species and the ortho and meta protons of the phenyl groups appear as two singlets (at 3.02 and 4.80 ppm for the *o*- and *o'*-H) and a doublet (at 3.95 and 4.20 ppm for *m*-H).

The above assignment of a low-spin iron(III) for the ((*p*-Et_2N)TPP)Fe(C_6H_5) species at room temperature appears to be in conflict with low-temperature ESR data of the same compound (Figure 2b). A low-spin assignment also appears to be in conflict with the "normal" trend expected for a spin equilibrium, i.e. low spin at low temperature and high spin at high temperature. This type of equilibrium between two spin states is highly unusual and to our knowledge has only been observed for a series of Co(II) salicylaldehyde Schiff base complexes where it is reported that the amount of high-spin series increased as the temperature decreased.[52] For the case of the iron σ-bonded species, the position of this spin equilibrium is very much dependent upon pressure, solvent conditions, and the phase (solid or liquid), indicating a large difference in entropic effects between the two different states. This will be the subject of a future publication.[26]

(50) Treichel, P. M.; Stone, F. G. A. In "Advances in Organometallic Chemistry"; Stone, F. G. A, West, R., Eds.; Academic Press: New York, 1964; Vol. I, p 143.
(51) Behere, D. V.; Birdy, R.; Mitra, S. *Inorg. Chem.* **1982**, *21*, 386.
(52) Migita, M.; Chirika, H.; Inaizumi, K. *J. Chem. Soc., Dalton Trans.* **1983**, 2281.

Scheme I

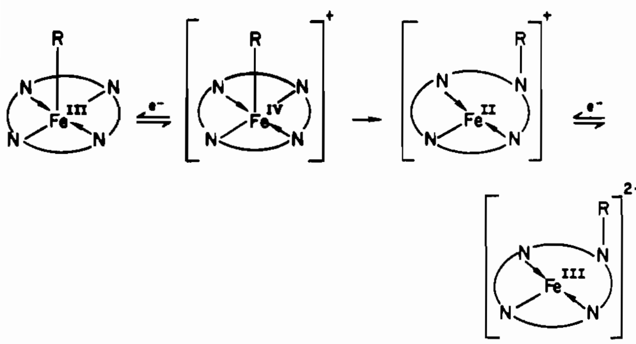

The ^1H NMR spectrum of $((CN)_4TPP)Fe(C_6H_5)$ is also typical of a low-spin iron(III) complex and agrees with the ESR data. The pyrrole protons exhibit a signal at −19.92 ppm, and resonance signals of the macrocyclic and axial ligands are comparable to those of the previously described σ-alkyl- and σ-aryliron(III) porphyrins. The ortho, meta, and para protons exhibit five separate signals located at higher fields than the corresponding unsubstituted tetraphenylporphyrin derivatives whose axial ligand is a perfluoroaryl group. Moreover, the ortho, para, and meta protons of the axial phenyl group are shielded compared to the corresponding $((p\text{-}Et_2N)TPP)Fe(C_6H_5)$ complex.

In summary, the effect of the electron-withdrawing perfluoro groups is to induce a displacement of the iron atom further away from the mean porphyrin plane so that a splitting of the d-orbital levels of the metal is diminished. Consequently, as described in the case of (TPP)FeCl,[51] occupancy of the d_{z^2} and the $d_{x^2-y^2}$ orbitals by unpaired electrons occurs, and ^1H NMR spectra of pure high-spin $S = {}^5/_2$ character are observed. This is in contrast to the $((CN)_4TPP)Fe(C_6H_5)$ species where a distortion of the z axis is predominant. Indeed, the V/Δ ratio of the rhombic and axial terms is around 0.36. The ratio has been calculated according to the method proposed by LaMar and Walker.[46] This distortion may be attributable to a lengthening of the iron d_{z^2} orbital and to a decreasing of the metal-macrocycle distance. This structural modification is due to the poor basicity of the equatorial ligand induced by the effect of the electron-withdrawing cyano groups. Moreover, the metal-to-nitrogen charge transfer resulting from the inductive effect of the cyano groups explains the presence of a superhyperfine structure on the ESR spectrum of $((CN)_4TPP)Fe(C_6H_5)$.

Electrochemistry of (P)Fe(R) Complexes. Previous investigations of $(TPP)Fe(C_6H_5)$ and $(OEP)Fe(C_6H_5)$ electrooxidations have characterized the overall electrode reaction as involving an ECE mechanism, leading to formation of an *N*-phenylporphyrin. This is shown by the general reaction sequence in Scheme I.[3]

A similar sequence of reactions also occurs for the tetracyano- and diethylamino-substituted complexes investigated in this study. Both of these complexes contain σ bonded phenyl groups and are low spin at room temperature. In contrast, the eight complexes containing σ-bonded C_6F_4H or C_6F_5 undergo a reversible one-electron oxidation, and no migration occurs on the spectroelectrochemical time scale. All of these complexes are high spin at room temperature. This is discussed in the following sections.

Electrochemistry of High-Spin $(P)Fe(C_6F_4H)$ and $(P)Fe(C_6F_5)$ Complexes. The eight high-spin perfluoro complexes were electrochemically investigated in PhCN (0.1 M $(TBA)PF_6$). Their half-wave potentials for oxidation and reduction are given in Table VI, and a representative voltammogram of $(TPP)Fe(C_6F_4H)$ is given in Figure 5a.

The $(TPP)Fe(C_6F_4H)$ and $(TPP)Fe(C_6F_5)$ complexes undergo three reductions and two oxidations within the potential limit of the electrochemical solvent. A similar number of reactions occurs for the substituted TPP complexes with perfluoro groups but is not observed for the OEP complexes due to solvent reduction at ∼−1.9 V. The first reduction is irreversible and occurs between −0.42 and −0.64 V depending upon the porphyrin ring. This reductive behavior is almost identical with that observed for the ionic (P)Fe(Cl) species in PhCN.[53] Additional similarities between the high-spin $(P)Fe(C_6F_4H)$ and (P)Fe(Cl) series are observed for the second reductions that (for a given porphyrin ring, P) occur at almost identical potentials in the range of −1.06 to −1.28 V (see Table VI). In contrast, the addition of a second electron to low-spin $(TPP)Fe(C_6H_5)$ and $(OEP)Fe(C_6H_5)$ is not observed in PhCN. The potential limit of this solvent is −1.9 V,

Table VI. Half-Wave Potentials of Different (P)Fe(R) and (P)Fe(Cl) Complexes in PhCN (0.1 M $(TBA)PF_6$)

porphyrin, P	axial ligand	spin state (room temp)	oxidn 2nd	oxidn 1st	redn 1st	redn 2nd	redn 3rd
OEP	Cl	hs		1.08	−0.54	−1.26	−1.95
	C_6F_5	hs	1.18	0.87	−0.59	−1.30	
	C_6F_4H	hs	1.14	0.79	−0.64	−1.28	
	C_6H_5[a]	ls	1.30	0.48	−0.93		
TPP	Cl	hs		1.14	−0.39	−1.09	−1.71
	C_6F_5	hs	1.38	0.94	−0.42	−1.06	−1.72
	C_6F_4H	hs	1.32	0.86	−0.45	−1.06	−1.71
	C_6H_5[a]	ls	1.43[c]	0.61	−0.70		
(*m*-Me)-TPP	Cl	hs	1.57	1.18	−0.33	−1.08	−1.73
	C_6F_5	hs	1.36	0.92	−0.42	−1.08	−1.76
	C_6F_4H	hs	1.31	0.84	−0.46	−1.06	−1.74
(*p*-Me)-TPP	Cl	hs	1.56	1.13	−0.34	−1.09	−1.77
	C_6F_5	hs	1.33	0.89	−0.45	−1.09	−1.77
	C_6F_4H	hs	1.28	0.82	−0.49	−1.07	−1.74
$(CN)_4TPP$	Cl[b]	hs		1.42[c]	0.16	−0.43	−0.85
	C_6H_5	ls		1.03	−0.03	−0.96	
(*p*-Et_2N)-TPP	Cl[b,d]	hs	0.73	0.59	−0.48	−1.17	
	C_6H_5[e]	ls	0.58	0.47	−0.83		

[a] From ref 3. [b] From ref 58. [c] E_{pa} at 100 mV/s. [d] Two additional oxidation waves were observed at 1.10 and 1.33 V. [e] Two additional waves were observed at 0.89 and 1.10 V.

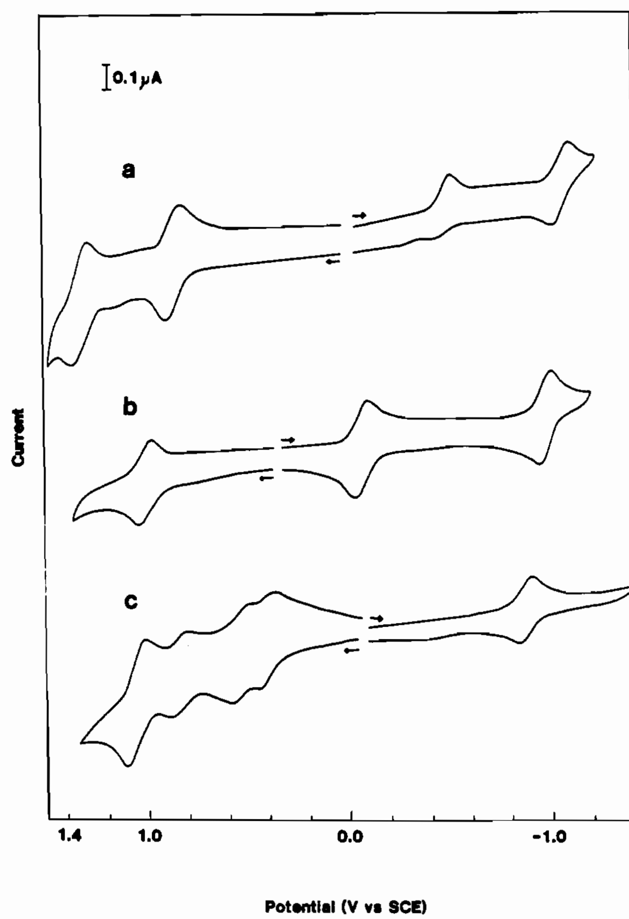

Figure 5. Cyclic voltammograms of (a) $(TPP)Fe(C_6F_4H)$, (b) $((CN)_4TPP)Fe(C_6H_5)$, and (c) $((p\text{-}Et_2N)TPP)Fe(C_6F_5)$, recorded in PhCN (0.1 M $(TBA)PF_6$) [scan rate 100 mV/s].

(53) Bottomley, L. A.; Kadish, K. M. *Inorg. Chem.* **1981**, *20*, 1348.

Table VII. Maximum Absorbance Wavelengths (λ_{max}) and Corresponding Molar Absorptivities (ϵ) of Neutral, Oxidized, and Reduced Forms of (TPP)Fe(Cl) and (TPP)Fe(C_6F_4H) in PhCN (0.3 M (TBA)PF_6)

compd	electrode reaction	λ_{max}, nm ($\epsilon \times 10^{-3}$)				
(TPP)Fe(C_6F_4H)	none	384 (38)	424 (91)	520 (10)	576 (6)	720 (5)
	1st oxidn		411 (63)	550 (20)		
	1st redn		435 (140)	539 (15)		
(TPP)Fe(Cl)	none	388 (41)	422 (95)	511 (14)	583 (2)	695 (4)
	1st oxidn		401 (52)	476 (20)	535 (19)	790 (5)
	1st redn		433 (137)	535 (13)		

and so any additional reductions beyond this potential are obscured by the reduction of the solvent.

As seen in Table VI, a 60-mV shift in $E_{1/2}$ is observed between the first reduction of (TPP)FeCl and the more difficult to reduce (TPP)Fe(C_6F_4H). The reversible half-wave potential for reduction of (TPP)Fe(C_6H_5) in PhCN is −0.70 V so that the magnitude of the potential shift between this species and the complex containing the σ-bonded C_6F_5 ligand is 280 mV. A similar difference of 340 mV is observed between the more difficult to reduce (OEP)Fe(C_6H_5) ($E_{1/2}$ = −0.93 V) and the more easily reducible (OEP)Fe(C_6F_5) ($E_{1/2}$ = −0.59 V). These potential shifts are not unexpected, however, and are predictable on the basis of differences in electron donor properties between the two σ-bonded R groups.

Reversal of the cathodic potential scan after the first reduction of (TPP)Fe(C_6F_4H) leads to the presence of an irreversible oxidation peak at 0.24 V. This potential is identical with that for the reversible oxidation of (TPP)Fe to generate (TPP)FeX (where X = PF_6^- or ClO_4^-)[53] and suggests cleavage of the iron–carbon bond after the initial one-electron reduction. The similarity of the second reduction potentials for the (P)Fe(C_6F_4H) and the (P)FeCl series also suggests loss of the σ-bonded ligand after the first electroreduction and agrees with both multiple-scan cyclic voltammetry in a bulk cell and thin-layer spectroelectrochemical investigations of this redox process.

Thin-layer cyclic voltammograms of (TPP)FeCl and (TPP)Fe(C_6F_4H) are represented in Figure 6a. The time-resolved spectra recorded after the first reduction of each complex show the same intense red-shifted Soret band and a single Q band as listed in Table VII. Reoxidation of the singly reduced species at a controlled potential of +0.4 V led to an identical spectrum for both the (TPP)Fe(C_6F_4H) and the (TPP)FeCl complex. Similar spectral and electrochemical behavior is also observed between the other perfluoro compounds and the corresponding (P)FeCl complexes, and on the basis of this similarity, the following mechanism (eq 1 and 2) is proposed for the first reduction and reoxidation of the (P)Fe(R) series where R = C_6F_4H and C_6F_5.

$$(P)Fe(R) \xrightarrow{e^-} [(P)Fe(R)]^- \rightarrow \rightarrow (P)Fe^{II} + [R]^{-\cdot} \quad (1)$$

$$(P)Fe^{II} + PF_6^- \rightleftarrows (P)Fe(PF_6) + e^- \quad (2)$$

The stability of oxidized high-spin (TPP)Fe(C_6F_4H) is quite different from that of oxidized low-spin (TPP)Fe(C_6H_5). This is shown in Figure 6a where the single-electron abstraction of the σ-bonded complex corresponds to reaction 3. The current–voltage

$$(TPP)Fe(C_6F_4H) \rightleftarrows [(TPP)Fe(C_6F_4H)]^+ + e^- \quad (3)$$

curves by cyclic voltammetry at a platinum electrode exhibit well-defined anodic and cathodic peaks where $E_p - E_{p/2}$ = 60 mV on the oxidative scans and i_{pa}/i_{pc} = 1.0. This same reversible diffusion-controlled behavior is observed on the thin-layer spectroelectrochemical time scale (30–60 s) where well-defined coupled anodic and cathodic peaks are obtained (Figure 6a).

The potential for reaction 3 varies between 0.79 and 0.94 V for oxidation of the eight different high-spin complexes, and for the case of (TPP)Fe(C_6F_5), this reaction occurs at 0.86 V. This value is between the observed potential for oxidation of high-spin (TPP)FeCl ($E_{1/2}$ = 1.14 V)[53] and that for oxidation of low-spin (TPP)Fe(C_6H_5) ($E_{1/2}$ = 0.61 V)[3] in the same solvent. The 330-mV positive shift in $E_{1/2}$ on going from low-spin (TPP)Fe(C_6H_5) to high-spin (TPP)Fe(C_6F_5) is in agreement with the

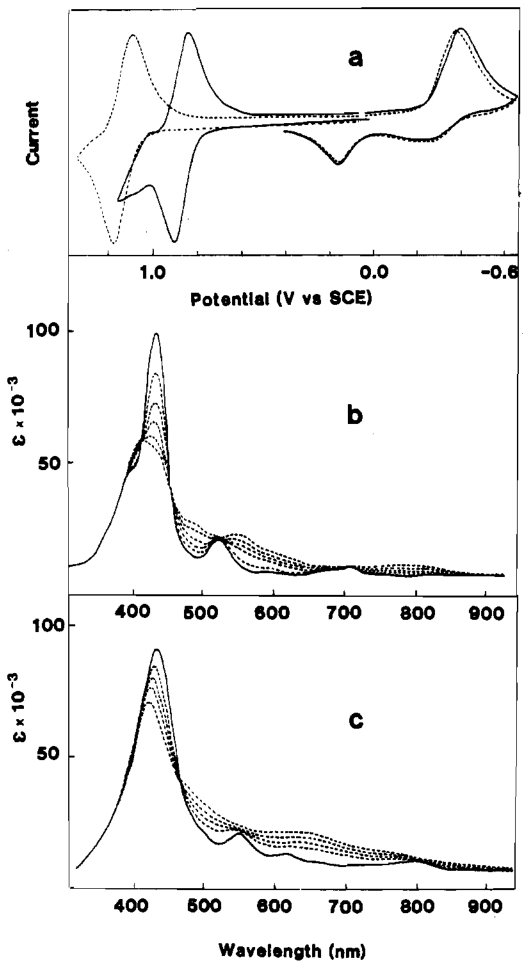

Figure 6. (a) Cyclic voltammograms of (TPP)Fe(C_6F_4H) (—) and (TPP)FeCl (- - -), at a platinum thin-layer electrode, in PhCN (0.3 M (TBA)PF_6) [scan rate 4 mV/s]. (b) Time-resolved electronic absorption spectra recorded during the oxidation of (TPP)Fe(C_6F_4H) at 1.3 V in PhCN (0.3 M (TBA)PF_6). (c) Time-resolved electronic absorption spectra recorded during the oxidation of (TPP)Fe(Cl) at 1.3 V in PhCN (0.3 M (TBA)PF_6). In all cases the initial species are represented by solid lines.

390-mV shift between low-spin (OEP)Fe(C_6H_5) ($E_{1/2}$ = 0.48 V) and high-spin (OEP)Fe(C_6F_5) ($E_{1/2}$ = 0.87 V) in PhCN and is simply accounted for by the increased electron-withdrawing effect of the C_6F_5 ligand with respect to that of C_6H_5. An 80-mV shift is observed between the first oxidation potentials of (P)Fe(C_6F_5) and (P)Fe(C_6F_4H). This is in accordance with a total difference of 390 mV between (OEP)Fe(C_6H_5) and (OEP)Fe(C_6F_5).

Of most significance in reaction 3 is the fact that the one-electron-oxidation product of the high-spin Fe(III) complex is stable on the thin-layer spectroelectrochemical time scale. This is shown in Figure 6b. For comparison purposes, time-resolved spectra recorded during oxidation of (TPP)FeCl at a controlled potential of +1.3 V in the same medium are also represented in Figure 6c and the wavelengths of the oxidized species are summarized in Table VII. As seen in Figure 6b,c similar qualitative decreases in peak intensity and maximum wavelength shifts toward lower wavelengths are observed for the two complexes. However,

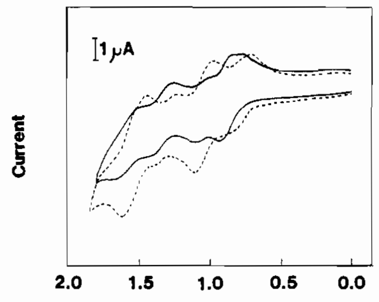

Figure 7. Cyclic voltammograms of (TPP)Fe(C_6F_4H) in PhCN (0.1 M (TBA)PF_6), after 4 min of electrolysis (—) at 1.0 V and after 12 min of electrolysis at 1.0 V (---) [scan rate 300 mV/s].

the final spectra obtained after the complete oxidation of the two species are significantly different. For (TPP)Fe(C_6F_4H), only a single broad peak is observed in the visible region (at 550 nm) and only weak absorption around 800 nm. Two clear isosbestic points are noted at 389 and 448 nm. After back-reduction at 0.0 V, the spectrum of the starting species is recorded. The significance of these spectral results for oxidized (TPP)Fe(C_6F_4H) is that no evidence for a following chemical reaction is observed. This is in contrast to the behavior of (TPP)Fe(C_6H_5) where the initial one-electron oxidation is followed by a rapid iron to nitrogen migration of the phenyl group to yield the $[(N\text{-}C_6H_5TPP)Fe^{II}]^+$ porphyrin[3] as shown in Scheme I.

Some evidence of a chemical reaction is presented at the much longer time scales of bulk coulometry (≈15 min). This is shown by the cyclic voltammograms obtained before and after bulk electrolysis of (TPP)Fe(C_6F_4H) at 1.0 V and by monitoring of the oxidized solution by ESR. Normal cyclic voltammograms of (TPP)Fe(C_6F_4H) show well-defined oxidation peaks at 0.86 and 1.32 V (as shown in Figure 5a). After bulk electrolysis for 4 min, these peaks begin to disappear and new peaks appear at 1.09 and 1.51 V. Finally, after 12 min of electrolysis three waves are clearly observed. The most significant of these peaks is at 1.09 and 1.54 V while a smaller set of peaks remains at $E_{1/2}$ = 0.84 V. This is illustrated in Figure 7. The species generated after the first oxidation at 1.0 V does not show any ESR signal. However, by changing the electrolysis potential to +1.2 V, a well-defined ESR spectrum was recorded after the abstraction of one electron. This spectrum is shown in Figure 8. The same ESR spectrum could also be obtained by abstracting two electrons in a direct controlled-potential oxidation at +1.2 V.

The resulting spectrum after the two-electron oxidation suggests a mixture of two ESR-active species, one at g = 1.99 and another with g values of 2.31 and 2.09. Formation of a cation radical as one of these species can be ruled out on the basis that coupling should occur between the Fe(III) center and the radical cation, resulting in an ESR-inactive species. On the other hand, the singly oxidized μ-oxo dimer $[((TPP)Fe)_2O]^+$ is known to have a sharp signal at g = 1.995 in CH_2Cl_2.[54,55] Therefore, the signal at g = 1.99 can reasonably be attributed to a small amount of this species which is formed as a side product during controlled-potential oxidation of (TPP)Fe(C_6F_4H). ESR signals of genuine $[(TPP)Fe]_2O$ give the same g values after electrolysis at +1.2 V but with an intensity 20 times higher than that shown in Figure 8. This suggests that the maximum amount of dimer formed as a side product is on the order of 5% and that the species with g values at 2.31 and 2.09 appears to be the main component in solution. This species is tentatively attributed to a low-spin Fe(III) dication. An alternate assignment of the ESR-active species as $[(N\text{-}C_6F_4H)PFe^{III}]^{2+}$ can be ruled out on the basis of the ESR spectrum that has none of the components expected for this type of species.

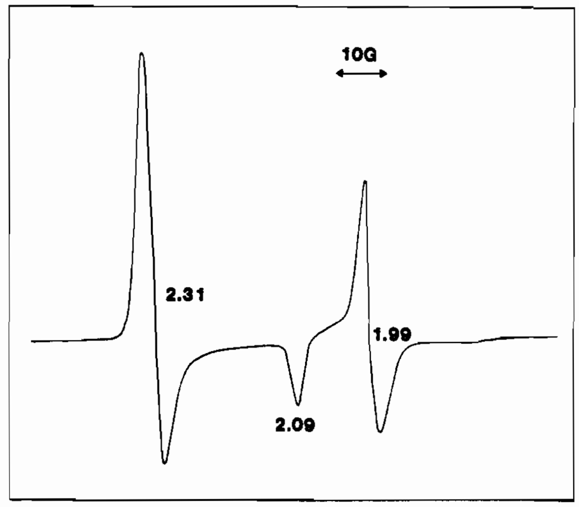

Figure 8. ESR spectrum of (TPP)Fe(C_6F_4H) after its two-electron oxidation at 1.2 V. Spectra were recorded at 115 K in CH_2Cl_2.

Electrochemistry and Spectroelectrochemistry of Low-Spin ((CN)$_4$TPP)Fe(C_6H_5) and ((*p*-Et$_2$N)TPP)Fe(C_6H_5). Cyclic voltammograms for the oxidation and reduction of low-spin ((CN)$_4$TPP)Fe(C_6H_5) and ((*p*-Et$_2$N)TPP)Fe(C_6H_5) are well-defined as shown in Figure 5b,c. For the former compound, in PhCN (0.1 M (TBA)PF_6) two reductions (at −0.03 and −0.96 V) and a single oxidation (at 1.03 V) are observed. All three reactions are diffusion controlled and exhibit theoretical peak separations of 60 ± 5 mV and values of i_{pa}/i_{pc} = 1.0. There is no evidence for loss of the phenyl group on the cyclic voltammetric time scale (although this does occur on longer time scales), and under these conditions the electrode reactions can be represented as in (4)–(6).

$$((CN)_4TPP)Fe(C_6H_5) + e^- \rightleftarrows [((CN)_4TPP)Fe(C_6H_5)]^- \quad (4)$$

$$[((CN)_4TPP)Fe(C_6H_5)]^- + e^- \rightleftarrows [((CN)_4TPP)Fe(C_6H_5)]^{2-} \quad (5)$$

$$((CN)_4TPP)Fe(C_6H_5) \rightleftarrows [((CN)_4TPP)Fe(C_6H_5)]^+ + e^- \quad (6)$$

The electroreduction of low-spin Fe(III) aryl or alkyl porphyrins has now been characterized for complexes with several different porphyrin ligands and σ-bonded alkyl or aryl groups,[3,4,12,13,37] and in all cases only a single reversible electrode reaction is observed in the potential range of the solvents. The fact that two single-electron additions can be observed for reduction of ((CN)$_4$TPP)Fe(C_6H_5) without cleavage of the phenyl group shows the remarkable stability of the iron–carbon σ bond and, for this complex, can be accounted for by the highly electron-withdrawing CN groups attached to the porphyrin macrocycle.

It is now well-known that the attachment of electron-withdrawing CN groups onto the macrocycle of a metallotetraphenylporphyrin leads to large positive shifts for oxidation and reduction of these complexes with respect to the unsubstituted complex.[40,56] For the case of ((CN)$_4$TPP)FeCl, and (TPP)FeCl reduction, these shifts range between 580 and 860 mV depending on the specific electrode reaction.[56,57] It is also known that the binding of a σ-bonded alkyl or aryl group to the iron center of a metalloporphyrin leads to large negative shifts of the reduction potential with respect to the same metalloporphyrin complex with ionic axial ligands, and for the case of (TPP)FeClO$_4$ and (TPP)Fe(C_6H_5) reduction, this shift amounts to 810 mV. Thus, perhaps it is not surprising that attachment of four CN groups to the porphyrin macrocycle and a σ-bonding phenyl group to the iron center of (TPP)Fe^{III} has a compensating effect such that the experimentally measured potentials (which reflect the electron

(54) Batten, P.; Hamilton, A. L.; Johnson, A. W.; Mahendran, M.; Wart, D.; King, T. J. *J. Chem. Soc., Perkin Trans.* **1977**, 1623.
(55) Felton, R. H.; Owen, G. S.; Dolphin, D.; Forman, A.; Borg, D. C.; Fajer, J. *Ann. N.Y. Acad. Sci.* **1973**, *206*, 504.
(56) Giraudeau, A.; Callot, H. J.; Gross, M. *Inorg. Chem.* **1979**, *18*, 201.
(57) Preliminary electrochemical results of ((CN)$_4$TPP)FeCl[40] were actually studies of the μ-oxo dimer. This was shown by a recent reinvestigation in our own laboratories.[58]

Table VIII. Maximum Absorbance Wavelengths (λ_{max}) and Corresponding Molar Absorptivities (ϵ) of Neutral, Oxidized, and Reduced Forms of $((p\text{-}Et_2N)TPP)Fe(C_6H_5)$, $((CN)_4TPP)Fe(C_6H_5)$ and $(N\text{-}C_6H_5)(p\text{-}Et_2N)TPPH$ in PhCN (0.3 M $(TBA)PF_6$)

compd	electrode reaction	λ_{max}, nm ($\epsilon \times 10^{-3}$)				
$((CN)_4TPP)Fe(C_6H_5)$	none		454 (95)	626 (42)		
	1st redn		446 (88)	582 (49)	711 (30)	
	1st oxidn		452 (78)	488 (65)	789 (30)	
	back-redn after 1st oxidn		451 (86)	656 (37)		
$((p\text{-}Et_2N)TPP)Fe(C_6H_5)$	none	388 (29)	452 (74)	529 (15)	675 (2)	
	1st redn	370 (27)	441 (89)	516 (17)	638 (4)	768 (2)
	1st oxidn		412 (7)	550 (25)	837 (27)	
$(N\text{-}C_6H_5)(p\text{-}Et_2N)TPPH$	none	412 (13)	486 (33)	583 (24)	804 (24)	
	1st oxidn		412 (7)	550 (26)	835 (29)	

density at a given reaction site) are very similar to those for (TPP)FeX.

In contrast to $((CN)_4TPP)Fe(C_6H_5)$, the half-wave potentials for oxidation or reduction of $((p\text{-}Et_2N)TPP)Fe(C_6H_5)$ are shifted in the same direction by the electron-donating diethylamino substituents and the σ-bonded phenyl group. This combined electron-donating effect from both the axial and the equatorial ligands results in a large negative shift of both the reduction and the oxidation potentials with respect to the simple $(TPP)Fe^{III}$ complex. This is shown in Figure 5c which illustrates a cyclic voltammogram of $((p\text{-}Et_2N)TPP)Fe(C_6H_5)$ in PhCN and in Table VI which summarizes the potentials for each of the electrode reactions.

As seen in Figure 5c, the electrochemistry of $((p\text{-}Et_2N)TPP)Fe(C_6H_5)$ is dominated both by the effect of the strongly electron-donating diethylamino groups and at the same time by the effect of the σ-bonded phenyl ligand. All previously studied complexes of diethylamino-substituted tetraphenylporphyrins have been characterized by multiple oxidation peaks of which the first two are significantly shifted in potential from the first two oxidation peaks of the respective unsubstituted metalloporphyrin.[58-61] For the case of $((p\text{-}Et_2N)TPP)FeCl$,[58] four oxidation processes are observed (at $E_{1/2}$ = 0.59, 0.73, 1.10, and 1.33 V), the first and second of which are shifted by 550 to 670 mV with respect to the first two oxidations of (TPP)FeCl (which occur at 1.14 and 1.40 V in the same solvent[53]). Thus, it is not surprising that four peaks are also observed for oxidation of $((p\text{-}Et_2N)TPP)Fe(C_6H_5)$. In this case, however, the second oxidation is shifted by 850 mV with respect to the second oxidation of $(TPP)Fe(C_6H_5)$ (E_{pc} = 1.31 V),[3] but for the first oxidation of these two complexes only a 140-mV difference in potential is observed. The last two oxidations of $((p\text{-}Et_2N)TPP)Fe(C_6H_5)$ occur at $E_{1/2}$ = 0.89 and 1.10 V which may be compared to similar peaks at 1.10 and 1.33 V for $((p\text{-}Et_2N)TPP)FeCl$.[58]

Two resonance forms have been suggested for $[(TPP)Fe(C_6H_5)]^-$ and $[(OEP)Fe(C_6H_5)]^-$ on the basis of their UV–visible spectra.[3] For these anionic complexes, absorptions between 700 and 800 nm were attributed to an anion-radical character of the species, while the presence of intense split red-shifted Soret bands were suggested to be indicative of Fe(II) contributions. This same resonance form might also be suggested for singly reduced $[((CN)_4TPP)Fe(C_6H_5)]^-$ and $[((p\text{-}Et_2N)TPP)Fe(C_6H_5)]^-$.

Only a single reduction peak is observed for $((p\text{-}Et_2N)TPP)Fe(C_6H_5)$. This reduction is reversible on the cyclic voltammetric and the thin-layer spectroelectrochemical time scales and gives rise to the spectrum shown in Figure 9a. This spectrum, whose molar absorptivities are given in Table VIII, shows an intense blue-shifted Soret band at 441 nm and three Q bands at 516, 638, and 768 nm. The first reduction of $((CN)_4TPP)Fe(C_6H_5)$ follows the same trend as depicted in Figure 9b. The final spectrum after controlled-potential reduction at −0.2 V shows a blue-shifted Soret band at 446 nm and two Q bands at 582 and 711 nm. In both cases, the spectra of the starting material were recovered after back-electrolysis at 0.0 V.

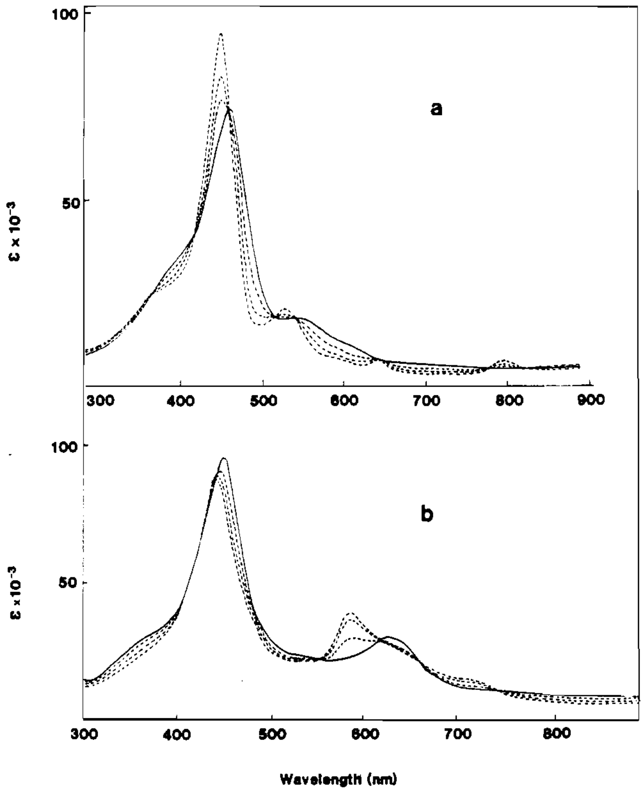

Figure 9. Time-resolved electronic absorption spectra taken at a platinum electrode during the reduction of (a) $((p\text{-}Et_2N)TPP)Fe(C_6H_5)$ at −1.1 V and (b) $((CN)_4TPP)Fe(C_6H_5)$ at −0.2 V, in PhCN (0.3 M $(TBA)PF_6$). Initial species are represented by solid lines.

The second reduction of $((CN)_4TPP)Fe(C_6H_5)$ occurs at −0.96 V in PhCN and does not lead to a well-defined spectrum. No shift was observed in the major absorption peaks, but a decrease in the intensity of the absorption was observed in the Soret and visible regions of the spectra. After reoxidation of the doubly reduced species at +0.3 V, the spectrum of the starting compound was recovered but with only half of its initial intensity. A probable explanation for this process is that the doubly reduced complex is only slightly soluble in PhCN and precipitates, thus decreasing the apparent molar absorptivity of the complex.

In oxidation, $((CN)_4TPP)Fe(C_6H_5)$ shows only one reversible wave (at 1.03 V) while $((p\text{-}Et_2N)TPP)Fe(C_6H_5)$ shows four reversible waves, three of which correspond to the abstraction of one electron (at 0.47, 0.58, and 0.89 V). The fourth wave (at 1.10 V) corresponds to the abstraction of two electrons. This is illustrated in Figure 5c. Unfortunately, we cannot record the spectra after all four oxidations of $((p\text{-}Et_2N)TPP)Fe(C_6H_5)$ since only the first oxidation wave may be recorded at the thin-layer spectroelectrochemical time scale. This wave appears irreversible in thin-layer oxidations, and upon reversal of the scan after that first oxidation, a new peak appears at +0.3 V. This is shown by time-resolved spectra that are represented in Figure 10a.

(58) Kadish, K. M.; Boisselier-Cocolios, B.; Simonet, B.; Chang, D.; Ledon, H.; Cocolios, P. *Inorg. Chem.* **1985**, *24*, 2148.

(59) Malinski, T.; Chang, D.; Bottomley, L. A.; Kadish, K. M. *Inorg. Chem.* **1982**, *21*, 4248.

(60) Chang, D.; Malinski, T.; Ulman, A.; Kadish, K. M. *Inorg. Chem.* **1984**, *23*, 817.

(61) Chang, D.; Cocolios, P.; Wu, Y. T.; Kadish, K. M. *Inorg. Chem.* **1984**, *23*, 1629.

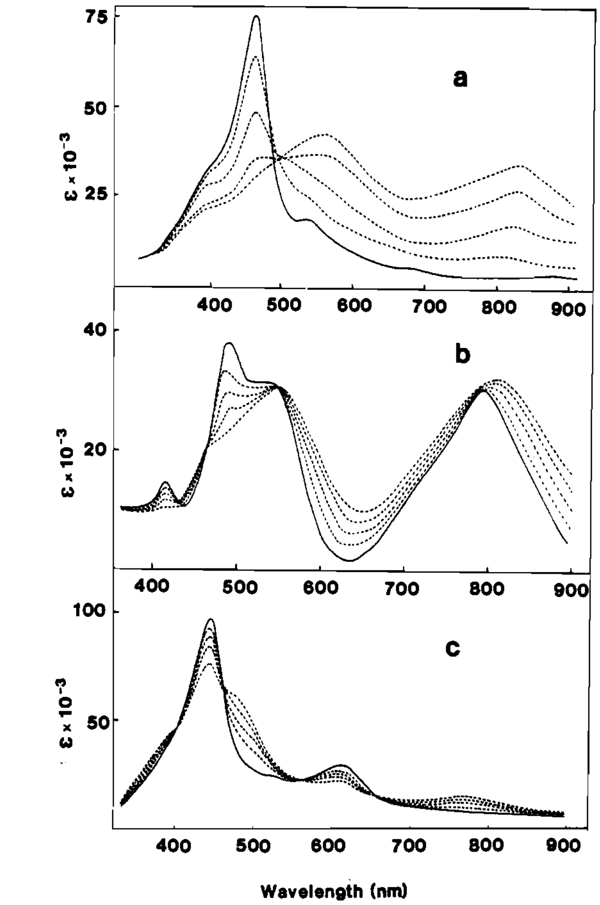

Figure 10. Time-resolved electronic absorption spectra taken at a platinum electrode during the oxidation of (a) $((p\text{-}Et_2N)TPP)Fe(C_6H_5)$ at +0.6 V, (b) $(N\text{-}C_6H_5)(p\text{-}Et_2N)TPPH$ at +0.6 V, and (c) $((CN)_4TPP)Fe(C_6H_5)$ at 1.3 V in PhCN, (0.3 M $(TBA)PF_6$). Initial species are represented by solid lines.

A disappearance of the Soret band is observed after electrooxidation of $((p\text{-}Et_2N)TPP)Fe(C_6H_5)$, and at the same time, two broad peaks appear at 550 and 837 nm. This spectrum has been identified as belonging to free base $(N\text{-}C_6H_5)(p\text{-}Et_2N)TPPH$, which is generated after migration of the phenyl group and demetalation. Assignment of the UV–visible spectra for this species was possible by an electrochemical study of genuine $(N\text{-}C_6H_5)(p\text{-}Et_2N)TPPH$ in the same media.[62] This free-base porphyrin was also identified by its NMR and IR spectra and exhibits a split Soret band and two intense and broad absorptions in the visible region. The cyclic voltammetry of this species exhibits one reversible oxidation wave at +0.3 V and a second irreversible one at +1.10 V. Time-resolved thin-layer spectra recorded at +0.6 V led to the same ill-defined spectrum recorded after oxidation of $((p\text{-}Et_2N)TPP)Fe(C_6H_5)$, i.e., a species characterized by two broad absorptions at 550 and 837 nm (Figure 10a).

The electrochemical oxidation of $((CN)_4TPP)Fe(C_6H_5)$ leads to a two-electron irreversible wave by thin-layer spectroelectrochemistry. The time-resolved UV-visible spectra recorded at 1.3 V show three isosbestic points in the oxidation, and no intermediate is detected in the process. This is illustrated in Figure 10c, and absorption maxima are listed in Table VIII. The generated species is reversibly reduced at 0.1 V. A second reduction also occurs at −0.45 V. However, even after two reductions, the final spectrum after back-electrolysis at 0.0 V never resembled the initial product. All of those spectral data lead us to suggest that the oxidation of low-spin $((CN)_4TPP)Fe(C_6H_5)$ is immediately followed by a rapid migration of the phenyl group as shown in Scheme I. This migration is irreversible.

Correlations between Spin State, Redox Potentials, and Stability of the Oxidized and Reduced Species. The results of this study indicate a direct correlation between the spin state of Fe(III) and the stability of the oxidized or reduced species. All of the high-spin species are unstable upon undergoing a one-electron reduction but are moderately stable upon being oxidized by one electron. This is in contrast to the low-spin σ-bonded C_6H_5 complexes. For these low-spin complexes the singly reduced species is extremely stable, but the singly oxidized species undergoes a rapid migration of the aryl group as shown in Scheme I.

The half-wave potentials for oxidation or reduction of (P)Fe(R) are directly influenced by the nature of the electron-donating or electron-withdrawing group on the porphyrin ring and/or the σ-bonded ligand. For example, each F group added to C_6H_5 contributes to an approximate 80-mV positive shift of potential. This is shown in Table VI. A similar positive shift is observed upon adding electron-withdrawing CN groups to the TPP of $(TPP)Fe(C_6H_5)$. For example, the difference between $(P)Fe(C_6H_5)$ where P = $(CN)_4TPP$ and P = TPP is 420 mV, with the former complex being the most difficult to oxidize.

It is tempting to relate the spin state and the stability of the oxidized Fe(III) species to the half-wave potential for electrooxidation. As seen in Table VI, the complexes having the most negative oxidation potential are low spin while those having the most positive oxidation potential are generally high spin. However, the most difficult to oxidize complex is $((CN)_4TPP)Fe(C_6H_5)$, and the most easy to oxidize complex is $(TPP)Fe(C_6H_5)$. Both of these species are low spin, and yet they bracket the range of potentials for oxidation of all of the high-spin complexes. This exception seems to rule against redox potentials as a sole criteria in determining spin state and product stability.

It is especially relevant to note that the high-spin complexes all undergo cleavage of the σ-bonded ligand after electroreduction. In contrast, the low-spin complexes are extremely stable after electroreduction. Again, this does not appear to be related to the potential of the reduction. The most difficult to reduce low-spin complex is $(OEP)Fe(C_6H_5)$, and this reduction occurs at −0.93 V. The most easy to reduce low-spin complex is $((CN)_4TPP)Fe(C_6H_5)$, and the first reduction of this compound occurs at −0.03 V. These reduction potentials bracket those of the high-spin derivatives.

It is significant to note the extreme stability of the Fe–carbon bond in the singly and doubly reduced low-spin complexes. For the case of low-spin $((CN)_4TPP)Fe(C_6H_5)$, the difference between the first and second reduction potential is 930 mV and no other reaction is observed up to the potential limit of the solvent. For the case of low-spin $(TPP)Fe(C_6H_5)$, a second reduction does not occur within the potential range of the solvent. Given a cathodic limit of −1.9 V, this would correspond to a difference of at least 1.2 V between the potential of the first and second reduction of $(TPP)Fe(C_6H_5)$ and of at least 1.1 V between the second and third reduction of $((CN)_4TPP)Fe(C_6H_5)$. This remarkable stability is not observed for any of the high-spin σ-bonded porphyrins investigated in this study.

Acknowledgment. The support of the National Institutes of Health (Grant GM25172) and the Robert A. Welch Foundation (Grant E-680) is gratefully acknowledged.

(62) Synthesis of $(N\text{-}C_6H_5)(p\text{-}Et_2N)TPPH$ was carried out by acid treatment of the corresponding $((p\text{-}Et_2N)TPP)Fe(C_6H_5)$. A benzene solution of phenylmagnesium bromide was added to 500 mg of $((p\text{-}Et_2N)TPP)Fe(Cl)$ (0.49 mmol) dissolved in 100 mL of benzene under argon, and the completion of the reaction was monitored by TLC. Hydrolysis was carried out with 50 mL of 5% H_2SO_4 in methanol, and air was bubbled through the reaction mixture for 3 h. The solution was then stirred overnight. After removal of methanol by washing with $NaHCO_3$, drying with Na_2SO_4, and evaporation of the solvent, the crude material was chromatographed in basic alumina. Elution with a 25:1 CH_2Cl_2/methanol mixture provide 21 mg (5%) of dark red crystals. ^1H NMR (C_6D_6, Me_4Si reference) δ: 0.96–1.47 (m, 24 H, Ph-*N*-$(CH_2\mathit{CH_3})_2$), 2.76 (d, 2 H, *N*-Ph, *o*-H), 3.55–3.76 (m, 16 H, Ph-*N*-$(\mathit{CH_2}CH_3)_2$), 4.90 (t, 2 H, *N*-Ph, *m*-H), 5.45 (t, 1 H, *N*-Ph, *p*-H), 7.08–7.25 (m, 8 H, meso-Ph, *m*-H), 7.74 (s, 2 H, 1,2-pyr H), 8.14–8.40 (m, 14 H, 3,4,7,8-pyr H, meso-Ph, *o*-H, 5,6-pyr H). IR (cm^{-1}): 1140, 1235, 765, 690. UV–visible (λ, nm ($\epsilon \times 10^{-3}$) (in PhCN)): 412 (13.3), 486 (33.1), 543 (24.2).

Registry No. (OEP)Fe(C_6F_4H), 96482-32-5; (TPP)Fe(C_6F_4H), 96482-33-6; ((*m*-Me)TPP)Fe(C_6F_4H), 96532-01-3; ((*p*-Me)TPP)Fe(C_6F_4H), 96482-34-7; (OEP)Fe(C_6F_5), 96502-36-2; (TPP)Fe(C_6F_5), 96502-37-3; ((*m*-Me)TPP)Fe(C_6F_5), 96502-38-4; ((*p*-Me)TPP)Fe(C_6F_5), 96532-02-4; ((*p*-Et_2N)TPP)Fe(C_6H_5), 96482-35-8; ((CN)$_4$TPP)Fe(C_6H_5), 96502-39-5; ((*p*-Et_2N)TPP)Fe(Cl), 85529-39-1; ((CN)$_4$TPP)Fe(Cl), 96293-36-6; (OEP)Fe(Cl), 28755-93-3; (TPP)Fe(Cl), 16456-81-8; ((*m*-Me)TPP)Fe(Cl), 52155-49-4; ((*p*-Me)TPP)Fe(Cl), 19496-18-5; C_6H_5Br, 108-86-1; C_6F_4HBr, 1559-88-2; C_6F_5Br, 344-04-7; (*N*-C_6H_5)(*p*-Et_2N)TPPH, 96502-40-8.

Contribution from the Department of Chemistry, Université Cadi-Ayyad, Marrakech, Morocco

Atropisomerism in Aryl-Substituted Borazines

S. ALLAOUD and B. FRANGE*

Received January 9, 1984

The *N,N',N''*-tri-*o*-tolylborazines (o-$CH_3C_6H_4NBX)_3$ (X = Cl, Br, Me, Et) were prepared and studied by means of ^{1}H and ^{13}C NMR. The methyl derivative (X = Me) resulting from the reaction of CH_3MgI on the *B,B',B''*-trichloro-*N,N',N''*-tri-*o*-tolylborazine (X = Cl) in diethyl ether was shown to be a mixture of the cis isomer alone with *B*-hydroxy byproducts that were identified. This methylation reaction fails to provide the expected trans isomer for steric reasons: instead, *B*-hydroxy compounds appear during the hydrolysis step.

Introduction

The fact that aromatic rings of *N,N',N''*-triaryl- (*B,B',B''*-triaryl-) substituted borazines are perpendicular to the plane of the borazine ring is strongly supported by several reports. Such evidence was first derived from ^{1}H NMR data on *N,N',N''*-triaryl-*B,B',B''*-trimethylborazines $(ArNBMe)_3$;[1] more recently, accurate structural analysis of $(C_6H_5NBCl)_3$ in the solid state led to a value of 77–87° for the angle between the phenyl substitutent and the borazine ring.[2] Furthermore, as a direct consequence of such a conformation for the phenyl group, partial separation of both expected isomers was achieved in the case of $(B$-o-Tol-NEt$)_3$, the identification being performed by means of ^{1}H NMR.[3] In the course of our systematic study of *N,N',N''*-triarylborazines, we were led to investigate from this standpoint the closely related *N,N',N''*-tri-*o*-tolylborazines (o-$CH_3C_6H_4NBX)_3$ (with X = Cl, Br, Me, and Et, respectively, for compounds I–IV) (Figure 1), using ^{1}H as well as ^{13}C and ^{11}B NMR; particular care was brought to the purification of the products by chromatographic methods (TLC and VPC). The results we have so far obtained are somewhat different from the above quoted;[3] in no case was it possible to provide evidence for atropisomerism in such systems.

Experimental Section

General Data. The solvents used were refluxed and distilled from CaH_2. Ethanol-free chloroform was obtained by passing spectrograde material through a short alumina column.[4] All reactions were carried out under a dry nitrogen atmosphere. NMR spectra were recorded on a Varian HT 80 spectrometer. The conditions were as follows: ^{1}H, 79.542 MHz, solvent $CDCl_3$, Me_4Si as internal standard, 5-mm-diameter tubes; ^{11}B, 25.517 MHz, solvent $CHCl_3$, boric acid as internal reference; ^{13}C, 20.000 MHz, solvent and reference $CHCl_3$ (chemical shifts converted to Me_4Si using $\delta_{Me_4Si} = \delta_{CHCl_3} + 77.2$ ppm). For the last two nuclei, spectra were run in 10-mm-diameter tubes, with a 5-mm coaxial tube containing D_2O for the lock and, eventually, the reference (boric acid). One ^{1}H NMR spectrum was recorded at 360 MHz on a Bruker WM 360, with $CDCl_3$ as a solvent. The following abbreviations were used to designate the multiplicity of the individual signals: s = singlet, d = doublet, t = triplet, m = multiplet, b = broad, dd = doublet of doublets, td = triplet of doublets. Infrared spectra were obtained as Nujol mulls on a Perkin-Elmer 735 B spectrometer. VPC was obtained on a Varian 1400 apparatus using a 1-m-long column filled with 10% OV 101 on Chromosorb GHP 100/120 mesh. TLC was performed on Merck silica gel 60 F 254 plates, and PLC, on Merck silicagel 60 plates (solvent C_6H_6). Melting points were determined on a Köffler melting point apparatus and are uncorrected.

***B,B',B''*-Trichloro-*N,N',N''*-tri-*o*-tolylborazine (I).** This compound was prepared according to established procedure[5] from BCl_3 and *o*-toluidine in toluene, the chlorobroazine recrystallizing from the solvent on cooling; yield 70%. ^{1}H NMR: 2.23 (s), 7.2 (m) ppm. ^{13}C NMR: aromatic CH 126.9, 128.1, 128.2, 128.3, 130.7, 131.0 ppm; CN 140 ppm; CCH_3 134 ppm; CCH_3 18.1 ppm.

***B,B',B''*-Trimethyl-*N,N',N''*-tri-*o*-tolylborazine (III).** To a diethyl ether solution of methylmagnesium iodide, prepared from magnesium turnings (1.09 g, 0.045 mol) and a slight excess of methyl iodide, was added *B,B',B''*-trichloro-*N,N',N''*-tri-*o*-tolylborazine (I) (5.68 g, 0.0125 mol) by small fractions, allowing a gentle boiling, and the mixture was refluxed 1 h. After cooling with an ice bath, the mixture was quenched with a solution of NH_4Cl and III was isolated by crystallization from an ether–methanol solution.[5] The yield of crude product was 3.24 g (66% based on I) of white crystals, mp 160–162 °C. TLC of the latter gives rise to three spots (C_6H_6 as eluent.) The same result was obtained by VPC (Figure 2) (oven temperature 280 °C, nitrogen 30 mL/min). Preparative TLC of the crude mixture yields the two main components: 0.080 g of *B,B',B''*-trimethyl-*N,N',N''*-tri-*o*-tolylborazine (III), mp 168–170 °C (lit.[6] mp 158–160 °C), as well as 0.020 g of the *B*-hydroxy derivative V, mp 163–165 °C. ^{1}H NMR of both compounds is reported (Figure 3). ^{13}C NMR for III: aromatic CH 125.1, 126.6, 128.2, 130.3 ppm; CCH_3 133.9 ppm; CN 147.4 ppm; CCH_3 18.3 ppm; BCH_3 1.4 ppm. ^{13}C NMR for V: aromatic CH 125.1, 125.8, 126.5, 126.6, 126.8, 126.85, 128.3, 128.4, 128.5, 130.3, 130.6 ppm; CCH_3 134.2, 134.7 ppm; CN 143.7, 147.2 ppm; CCH_3 18.1, 18.3 ppm.

***B,B',B''*-Triethyl-*N,N',N''*-tri-*o*-tolylborazine (IV).** To an ether solution of ethylmagnesium iodide (0.045 mol) was added solid *B,B',B''*-trichloro-*N,N',N''*-tri-*o*-tolylborazine I (5.68 g, 0.0125 mol), and the mixture was refluxed for 1 h. After hydrolysis (NH_4Cl method), IV was isolated and then purified by recrystallization from an ether–ethanol solution. The yield of IV was 2.44 g (45% based on I) of white crystals, mp 130–135 °C (lit.[3] mp 130–132 °C). From the ^{1}H NMR spectrum, it may be concluded that the product is also contaminated by *B*-hydroxy derivatives, but isolation of pure compounds by PLC was unsuccessful. Furthermore, small amounts of unidentified impurities were detected by VPC.

2,4-Dibromo-3-*o*-tolyl-8-methyl-2,4-dibora-1,3-diazanaphthalene (VII). The reaction of boron tribomide BBr_3 (34.43 g, 0.137 mol) with *o*-toluidine (14.85 g, 0.1385 mol) in boiling chlorobenzene, under nitrogen, does not lead to the expected bromoborazine, II, but to the title compound VII in a nearly quantitative yield. After concentration of the solution, 14.25 g of VII (yield 53%) was obtained as yellow crystals most sensitive to moisture. ^{1}H NMR= CCH_3 2.10 (s), 2.40 (s) ppm; aromatic CH 7.4 (m), 7.92 (d) ppm. ^{13}C NMR: aromatic CH 121.7, 126.7, 126.9, 127.9, 130.5, 134.9, 136.0 ppm; CCH_3 122.8, 133.7 ppm; CN 145.2, 145.3 ppm; CCH_3 16.8, 18.5 ppm. Anal. Calcd for $C_{14}H_{14}N_2$-

(1) I. M. Butcher, W. Gerrard, J. B. Leane, and E. F. Mooney, *J. Chem. Soc.*, 4528 (1964).
(2) W. Schwarz, D. Lux, and H. Hess, *Cryst. Struct. Commun.*, **6**, 431 (1977).
(3) P. M. Johnson and E. K. Mellon, *Inorg. Chem.*, **13**, 2769 (1974).
(4) "Vogel's Textbook of Practical Organic Chemistry", 4th ed., Longmans, Green and Co., London and New York, 1978, p 268.
(5) S. J. Groszos and S. F. Stafiej, *J. Am. Chem. Soc.*, **80**, 1357 (1958).
(6) W. Gerrard, E. F. Mooney, and D. E. Pratt, *J. Appl. Chem.*, **13**, 127 (1963).

0020-1669/85/1324-2520$01.50/0